Chapter 14
Rapid Integration Across Tonotopy by Individual Auditory Brainstem Octopus Cells

Matthew J. McGinley

Abstract Broadband transient sounds, such as clicks, are transduced in a traveling wave in the cochlea that spreads from base to apex. This traveling wave causes delays in the activation of auditory nerve fibers that vary systematically as a function of the tonotopy in the ventral cochlear nucleus (VCN) in the brainstem, activating high-frequency fibers first. Octopus cells in the mammalian VCN consistently spread their dendrites across the tonotopic axis so that the tips receive input from fibers tuned to the highest frequencies. As a result, broadband transient sounds produce a somatopetal (soma-directed) sweep of activation in octopus cells' dendrites. Low-voltage-activated potassium channels (g_{KL}) in the dendrites and soma sharpen the sensitivity to sweep duration. Branch points in octopus cells' dendrites show significant impedance mismatch, resulting in violation of Rall's "3/2 power law" and shaping of sweep sensitivity. Thus, the morphology, connectivity, and membrane biophysics of octopus cells allow them to compensate for the cochlear traveling wave delay and respond to clicks with exquisite temporal precision. In the context of the time–frequency (Gabor) uncertainty principle, octopus cells can be seen to solve a general problem of encoding frequency-dispersed but temporally restricted patterns using somatopetal sweep sensitivity. Compensation for longer delays in low-frequency hearing animals, implications for downstream processing, and relationship to other systems are discussed.

M.J. McGinley, Ph.D. (✉)
Neurobiology Department, School of Medicine, Yale University,
333 Cedar Street, New Haven, CT 06510, USA
e-mail: matthew.mcginley@yale.edu

14.1 Temporally Precise Coding: The Problem of Broadband Transients

Speed and temporal precision are at the heart of auditory processing. Auditory nerve fibers (ANFs) in mice can detect sound pressure fluctuations with periods as short as 12 μs (Taberner and Liberman 2005), and humans can detect differences of as little as 10 μs in the time of arrival of a sound between the ears (Mills 1958). By contrast, sensory systems that rely on G-protein-coupled receptors, such as vision and olfaction, process information ~10,000 times more slowly (Hille 1994). The phenomenal speed of mammalian auditory systems is made possible by the precise transduction of sound pressure waves in air into a traveling wave down the basilar membrane in the cochlea (Fig. 14.1a). This traveling wave performs a spectral decomposition into a spatial frequency map along a logarithmically spaced frequency axis (Dallos 1992). The cochlea can thus be thought of as a log-spaced parallel bank of band-pass filters (Yang et al. 1992) with exquisite temporal and frequency resolution that approaches the physical limits of sound (Weisburn and Parks 1992).

Temporal precision in the processing of broadband sounds presents a special problem to auditory systems. In the filter bank model of the cochlea, for each frequency channel (i.e., each hair cell or ANF) there is an inherent trade-off between its spectral and temporal resolution, encapsulated by the Gabor uncertainty principle (Gabor 1946): $\Delta t \times \Delta f \geq 1/\pi$; Δt is the uncertainty in time, and Δf is the uncertainty in frequency, originally inspired by the Heisenberg uncertainty principle (Heisenberg 1927). Simply put, it takes time to determine the frequency of an oscillation with precision. As a result of this trade-off, the uncertainty in, for example, the time of onset of each spectral component of a broadband sound is inversely related to the uncertainty in the frequency of that component. Since the uncertainty in frequency is related to the frequency itself (approximately proportional to the log of the frequency) (Taberner and Liberman 2005), the temporal uncertainty varies systematically with the frequency of the sound component.

The cochlear traveling wave can thus be viewed as a particular solution to the Gabor uncertainty problem. This idea can be tested by analyzing the timing of firing of the first action potential by an ANF in response to a click sound (Fig. 14.1b). The latency from tone onset to first action potential consists of a constant delay, T_c, reflecting the acoustic system, axonal propagation, etc., and a group delay that varies with the sound frequency, $T(f)$, corresponding to the traveling wave delay. The total delay is the sum of the two: $T_t = T_c + T(f)$. From the Gabor uncertainty perspective, $T(f)$, the frequency-dependent delay, is equal to the uncertainty in the time of the signal, Δt. Equating these terms makes the assertion that the group delay at each frequency reflects an accumulation of evidence overcoming the temporal uncertainty, after which time an action potential codes the occurrence of sound energy in that frequency channel. Next, we assume that the uncertainty in frequency, Δf, is proportional to the log of the frequency, reflecting the log-based spacing of the cochlear
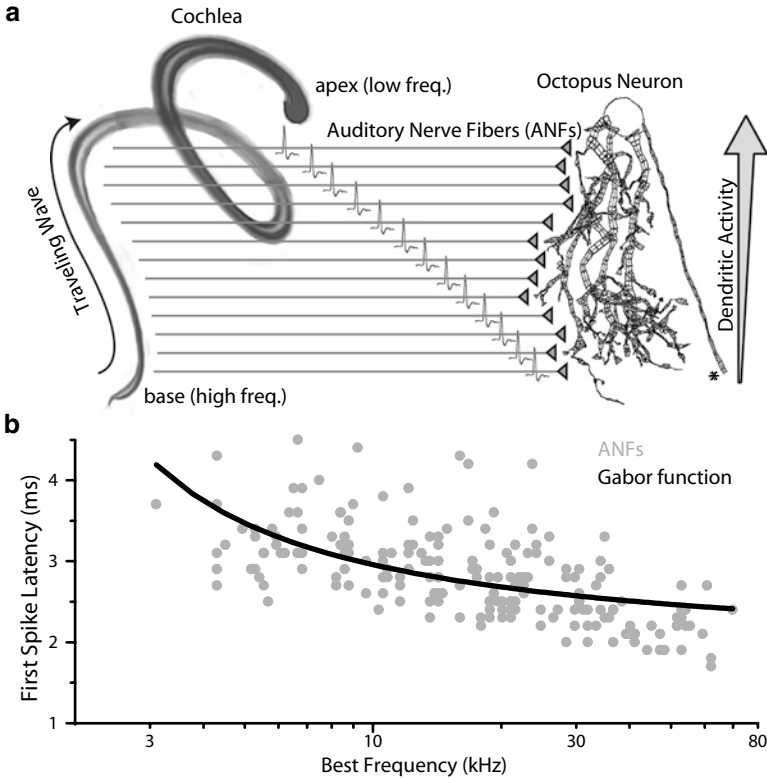
Fig. 14.1 The cochlear traveling wave delay results in a somatopetal wave of activation down the dendrites of octopus cells. (**a**) A schematic representation of the traveling wave spreading down the basilar membrane of the cochlea of a mouse from base to apex (*left*) resulting in a delay line in the activation of auditory nerve fibers (*middle*). This delay profile results in a somatopetal wave of dendritic activity in the dendrites of octopus cells in responses to broadband transient sounds. The *asterisk* indicates the axon of the reconstructed octopus cell. (**b**) The traveling wave delay in mice is apparent in first-spike latencies in responses recorded in vivo to clicks. The *black curve* is the result of a least-squares regression fit of the Gabor uncertainty function ($T_c = 1.8 \pm 0.1$ ms and $\alpha = 0.36 \pm 0.04$). Parts of panels (**a**) and (**b**) are reproduced with permission from Fig. 14.1 of ref. McGinley et al. (2012)

filter bank. Substituting the uncertainty relationship into the equation for total delay yields $T_t = T_c + \dfrac{1}{\left(\pi \times \alpha \times \ln(f) \right)}$, where α is the proportionality constant.

A fit to the first spike latency data with a delay function derived from the Gabor uncertainty relationship is in reasonably good agreement with the data (Fig. 14.1b). In particular, it captures the tendency of traveling wave delays to be proportionately larger at lower frequencies, corresponding to the slowing of the traveling wave as it approaches the apex of the cochlea. This slowing effect is prominent in animals with low-frequency hearing (Ruggero 1992). A better prediction would be

generated by incorporating the experimentally measured frequency dependence of sharpness of tuning of ANFs (e.g., ref. Taberner and Liberman 2005, Fig. 14.3b) into the function for frequency uncertainty, rather than assuming a linear dependence on log frequency.

Whether viewed as a solution to the Gabor uncertainty problem or simply as a temporal dispersion, the cochlear traveling wave delay, which lasts 1.6 ms in mice (McGinley et al. 2012) and up to 8 ms in animals with low-frequency hearing, including humans (Ruggero and Rich 1987), results in asynchronous activity in the population of auditory nerve fibers in response to broadband transient sounds. This asynchrony must be dealt with by downstream neurons or circuits if broadband transient sounds are to be encoded precisely, for example to signal the snapping of a branch under the foot of a predator.

14.2 Biophysical Specializations of Octopus Cells: Built for Speed

From the cochlea, ANFs project their axons to the cochlear nucleus where they synapse on several classes of principal neurons that in turn carry acoustic information to the next stage of the auditory pathway (Fig. 14.1a). One of the principal classes, octopus cells, is in all respects built for speed. They have extraordinarily brief membrane time constants (~300 μs) and low input resistances (~5 MΩ) (Golding et al. 1995, 1999), making them perhaps the fastest neurons in the mammalian brain (Spruston et al. 2007). Their fast membranes result from a high density of low-voltage-activated potassium conductance (g_{KL}) and hyperpolarization-activated, cyclic nucleotide-gated, channels in their soma and dendrites (Oertel et al. 2008), which oppose each other in a balance at the resting potential (Bal and Oertel 2000, 2001; Cao and Oertel 2011). Octopus cells also have brief synaptic currents, mediated through rapid calcium-permeable AMPA receptors (Gardner et al. 1999, 2001; Raman and Trussell 1992). Octopus cells express voltage-gated calcium channels (Golding et al. 1999; Bal and Oertel 2007), but their physiological role is not known. There is an atypical developmental profile of cholinergic receptors in octopus cells, which may influence their intracellular calcium dynamics (Morley and Happe 2000).

The high density of g_{KL} channels in octopus cells results in an unusual action potential generation mechanism. If an octopus cell is depolarized slowly, g_{KL} channels open, shunt the sodium current, and prevent the generation of an action potential (Fig. 14.2a). If instead an octopus cell is depolarized quickly, g_{KL} channels do not have time to open, creating a window for sodium channel activation to cause an action potential (Fig. 14.2a). Thus, octopus cells have a threshold in rate of depolarization or dV/dt (Fig. 14.2b, left) (Ferragamo and Oertel 2002; Cai et al.

1997). This dV/dt threshold is a feature of other auditory neurons with high g$_{KL}$, including bushy cells (McGinley and Oertel 2006) and neurons in the medial superior olive (Golding and Oertel 2012; Cai et al. 2000), which have intrinsic membrane properties that are very similar to octopus cells. The dV/dt threshold creates an integration window or time during which somatic depolarization must occur to result in an action potential (McGinley and Oertel 2006), which results in extremely stringent coincidence detection (Oertel et al. 2009; Golding and Oertel 2012; König et al. 1996). The integration window in octopus cells is ~1 ms (Fig. 14.2b, right) (McGinley and Oertel 2006).

As a result of the dV/dt threshold, excitatory postsynaptic potentials (EPSPs) in octopus cells must rise quickly in order to elicit an action potential. EPSPs must also result in sufficient depolarization to activate sodium channels, and thus octopus cells also have a voltage threshold. The relationship between the rate-of-depolarization threshold and the voltage threshold for an action potential has not been explored. Determining the function describing this relationship, $V_{thresh}(dV/dt)$, would provide a more complete picture of the input–output relationship of neurons with a dV/dt threshold. Furthermore, knowing this relationship would motivate a natural definition of the efficacy of a composite EPSP waveform:

$$\varepsilon_{syn} = \begin{cases} A_{syn} \,/\, (V_{thresh}\left(dV_{syn}\right) - V_{rest}) & if\ dV_{syn} \geq dV\,/\,dt_{thresh} \\ 0 & if\ dV_{syn} < dV\,/\,dt_{thresh} \end{cases}$$

where A_{syn} is the EPSP amplitude and dV_{syn} is the rate of depolarization during the rising phase of the EPSP. Visual inspection of the voltage response to current ramps suggests that the voltage threshold does not change dramatically with rate of depolarization (Fig. 14.2a). Therefore, the amplitude of an EPSP is a reasonable first approximation to its efficacy when the rate of rise is above dV/dt threshold. Steady depolarization—which may arise from ongoing synaptic activity or modulatory influences—does not affect the dV/dt threshold, at least in bushy cells (McGinley and Oertel 2006). However, it may affect the voltage threshold (Levy and Kipke 1998), also warranting further investigation.

Octopus cells put their extraordinary speed to use when processing sounds. They respond rapidly and with great temporal precision to onset transients in broadband sounds such as clicks or in loud narrowband sounds. In cats, they respond with sub-millisecond temporal precision to clicks (Godfrey et al. 1975), having a jitter that is less than 200 µs during a 500 Hz click train (Oertel et al. 2000), and can fire at every cycle of a loud 800 Hz tone (Rhode and Smith 1986). They encode rapid temporal components of vocalizations by strongly phase locking to the fundamental frequency in the presence of formants (Rhode 1998) and to the signal envelope of rapid amplitude modulations (Rhode 1994), which are prominent in speech and music.

They may contribute to pitch representation, which occurs explicitly in primary auditory cortex by unexplained mechanisms (Rhode 1995; Bendor and Wang 2005). Thus, octopus cells respond with temporal precision to broadband transients in sounds in a variety of contexts, despite the cochlear traveling wave delay. The sound responses and cellular and synaptic biophysics of octopus cells have been reviewed in detail elsewhere (Oertel et al. 2000, 2009; Golding and Oertel 2012).

14.3 Morphology and Connectivity of Octopus Cells: Positioned to Integrate Broadband Sounds

Octopus cells were named on the basis of their striking morphology; they have several thick primary dendrites that emanate and branch from only one side of the cell body (Fig. 14.2c) (Osen 1969). Octopus cells also have thick daughter branches throughout their dendritic trees. This can be seen when comparing the diameter of parent and daughter branches to the so-called 3/2 power law of Rall: $d_p^{3/2} = d_{d,1}^{3/2} + d_{d,2}^{3/2}$, where d_p is the diameter of the parent dendrite, and d_d "1" and "2" are the diameters of the daughter dendrites at a branch point (Rall 1964). If a branch point obeys this power law, the impedance at the branch will be matched. Octopus dendritic branch points consistently violate the power law, with the right side of the equation being larger than the left for nearly all branches due to large daughter branches (see ref. McGinley et al. 2012, Fig. 8d). This could serve several functions for octopus cell dendritic integration, including increased distal dendritic surface area, rapid transmission of dendritic signals, or delays due to impedance mismatch.

The tendency of thick daughter dendrites to increase distal dendritic surface area can be seen in a simple box representation of octopus cell morphology; substantial surface area is distributed across many branch orders (Fig. 14.2d). Since the surface area of a cylinder is linearly proportional to its diameter, branches obeying the 3/2

Fig. 14.2 (continued) each action potential is indicated with an *asterisk* symbol. (**b**) The dV/dt threshold and integration window vary between several principal cell types of the VCN. Octopus cells have higher dV/dt thresholds and shorter integration windows than bushy cells. Stellate cells exhibit classical "integrator" characteristics. They do not have a dV/dt threshold, so their integration window is not limited by the action potential generation mechanism. (**c**) Photomicrograph of a biocytin-labeled octopus cell against a Nissel stain background (*left*) and 3D digital reconstruction of the same neuron (*right*). *D* dorsal; *M* medial. (**d**) A *box* representation of the dendritic morphology of octopus cells. Each *box* corresponds to a branch order. The *x*-axis is length, and the *y*-axis is total surface area. Each *box* is the average across cells of the average across branches within each order for each cell. The *oval* corresponds to the soma; the *x*-axis is the diameter, and the *y*-axis is the surface area of a sphere with equivalent surface area to a reconstruction of the soma. Panel (**b**) is reproduced with permission from Fig. 5 of ref. McGinley and Oertel 2006 and panels (**c**) and (**d**) from Fig. 8 of ref. McGinley et al. (2012)
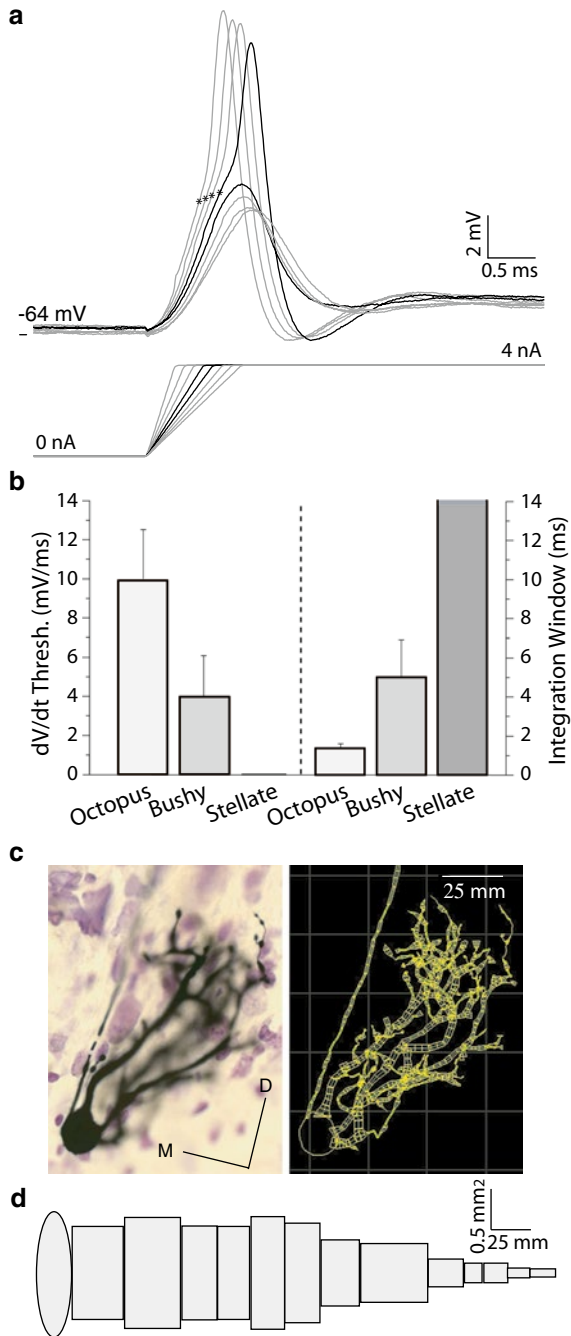
Fig. 14.2 The unique biophysics and morphology of octopus cells. (**a**) The membrane voltage of an octopus cell (*top*) during application of linear current ramps of varying durations (*bottom*). *Black traces* show the membrane voltage just below and above the rate-of-depolarization (d*V*/d*t*) threshold. Longer duration subthreshold ramps do not trigger an action potential (not shown; see refs. Morley and Happe 2000; Cai et al. 1997). The visually determined approximate voltage threshold for

power law would distribute less surface area into their daughter dendrites. Thick daughter dendrites could increase the speed of signal transmission by reducing the axial resistance, whereas the impedance mismatch at branch points would delay propagation from smaller to larger diameter dendrites (Agmon-Snir and Segev 1993; Lanzinger 1987). The original study demonstrating that octopus cells compensate traveling wave delays predicted a delay compensation of ~0.5 ms, matching in vivo delays measured in the same species (McGinley et al. 2005, 2012). A more recent study that did not incorporate detailed morphological information predicted compensation for about half of that delay (~0.28 ms) (Spencer et al. 2012), suggesting that the precise morphology is important.

The dominant source of synaptic input to octopus cells is excitation from the auditory nerve (Oertel et al. 2000). ANFs are tonotopically organized in the cochlear nucleus of all mammals studied, including mice (Osen 1970; Wickesberg and Oertel 1988). Octopus cells orient their dendrites across the tonotopic axis, so ANFs that encode higher frequencies synapse closer to the tips of the dendrites, and those that encode lower frequencies synapse closer to the soma (Fig. 14.1a, see also ref. Golding et al. 1995). Octopus cells show some diversity in morphology (Rhode et al. 1983) and, in mice but not cats, excite one another through axon collaterals (Golding et al. 1995), serving unknown functions in the processing of sounds (Godfrey et al. 1975; Rhode et al. 1983).

The role of inhibitory connections onto octopus cells is uncertain but may be minimal. Stimulation of the auditory nerve does not elicit GABAergic or glycinergic inhibition in octopus cells in mice (Golding et al. 1995). Consistent with this observation, there is a marked lack of glycinergic staining in the octopus cell area (Wenthold et al. 1987; Wickesberg et al. 1994), and tuberculoventral glycinergic interneurons exclude their projection from the octopus cell area (Wickesberg et al. 1991). However, GABAergic terminals exist on octopus cell dendrites (Marie et al. 1989), and glycine may be expressed in terminals in the octopus cell area of guinea pigs (Kolston et al. 1992), though glycine expression is sensitive to experimental conditions (Wickesberg et al. 1994).

14.4 Rapid Integration Across Tonotopy: A Marriage of Morphology and Connectivity with Biophysics

The relationship of tonotopy in the cochlear nucleus (Osen 1970) with the dendritic morphology of octopus cells (Osen 1969) led to early speculation about their role in sound processing. It was suggested that octopus cells' dendritic orientation might determine the sensitivity to frequency-modulated (FM) sweeps of different rates or direction (Morest et al. 1973). This idea was later related to Rall's developing view of spatiotemporal integration in dendrites (Szentagothai and Arbib 1974). The discovery in mice that octopus cells orient their dendrites in a consistent orientation

and direction with respect to the tonotopic organization led to the hypothesis that octopus cells compensate the traveling wave delay in their dendrites (Golding et al. 1995; Wickesberg and Oertel 1988).

This hypothesis was directly tested in mice by combining in vivo measurements of the traveling wave delay, in vitro recordings from octopus cells, morphological reconstruction, and passive and active compartmental modeling (McGinley et al. 2012). The traveling wave delay was measured in mice and found to be ~1.6 ms across the full hearing range (see Fig. 14.1b). Because octopus cells' dendrites span about 1/3 of the tonotopy in the VCN (Golding et al. 1995), during a broadband transient sound each neuron will be exposed to an ~0.5-ms sweep of dendritic activation spreading somatopetally (towards the soma) (see Fig. 14.1a). In separate experiments, whole-cell recordings in the current-clamp configuration were made from octopus cells in acute slices of the VCN from mice. Families of current steps were applied to determine the passive and active response of the membrane (Fig. 14.3a, b, black traces). After fixation, morphological reconstructions were made of recorded neurons (Fig. 14.2c, left) and imported into the software NEURON (Hines and Carnevale 1997) for computation modeling (Fig. 14.2c, right).

Passive compartmental models of octopus cells were built from current-clamp recordings and morphological reconstructions, using simulated annealing (Kirkpatrick and Vecchi 1983) to optimize fits of the models to the data (Fig. 14.3a). Active models were constructed using a model of the low-voltage-activated potassium conductance (g_{KL}) derived from medial superior olive neurons (Khurana et al. 2011), which have very similar g_{KL} channels to octopus cell neurons (Golding and Oertel 2012; Bal and Oertel 2001; Scott et al. 2005; Mathews et al. 2010), and a model of hyperpolarization-activated, cyclic nucleotide-gated channels derived from octopus cells (Bal and Oertel 2000; McGinley et al. 2012). Model parameters were adjusted for each model to result in a close match to the current-clamp recordings from the modeled neuron (Fig. 14.3b). Because g_{KL}- and hyperpolarization-activated channels are known to reside in the dendrites of octopus cells and medial superior olivary neurons (Scott et al. 2005; Mathews et al. 2010; Oertel et al. 2008), these channels were included in the dendrites in active models. The kinetics of excitatory synaptic conductances were set to match previous recordings from octopus cells (Gardner et al. 1999).

To test the sensitivity of octopus cells to somatopetal sweeps of synaptic activation arising from the traveling wave delay, the waveform of the somatic EPSP was determined in passive and active models in response to somatopetal sweeps of excitation with different durations. A single-compartment (point) model with identical input resistance and membrane time constant to each passive model was compared in order to evaluate the role of dendrites in shaping the somatic EPSP. Comparison was also made to a passive model with the location of arrival of each input randomized in order to evaluate the role of tonotopy and the resulting somatopetal wave of activation in EPSP shape. A final model was generated with the magnitude of the synaptic conductance at each dendritic location adjusted so that the somatic EPSP in response to individual synaptic activation was approximately constant. Such
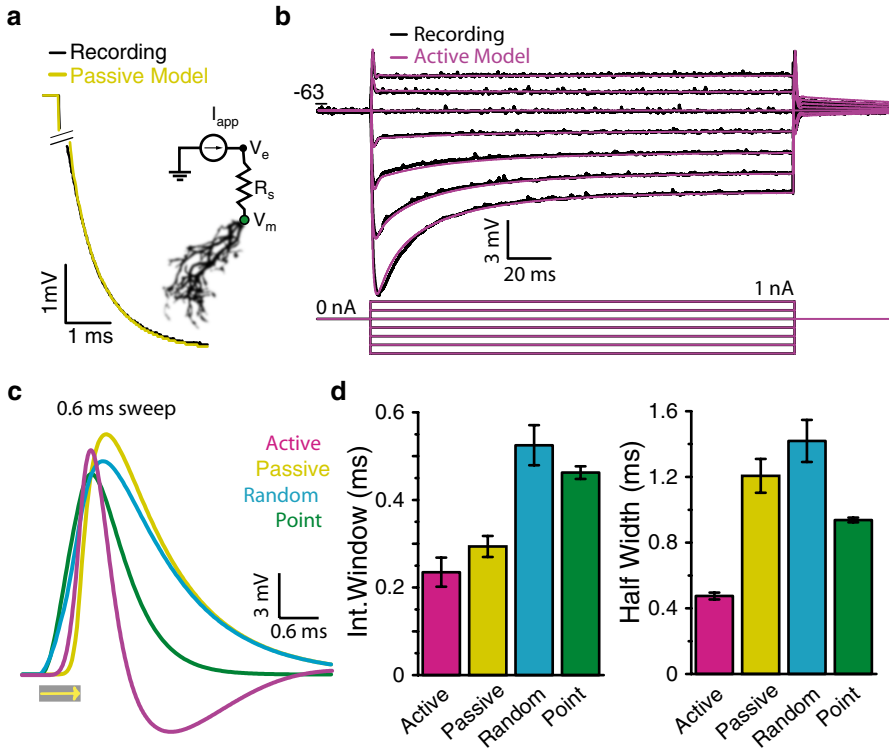
Fig. 14.3 Sensitivity to somatopetal sweeps of synaptic activation in biophysically and morphologically realistic models of octopus cells. (**a**) An example recording corrected for I_h (*black curve*) and the superimposed best-fit passive simulation (*yellow curve*). The series resistance drop, indicated by the *break*, was removed. The *inset* shows a diagram of the circuit used in passive simulations: I_{app} applied current; V_e electrode voltage; R_s series resistance; V_m membrane voltage. (**b**) Response of an octopus cell (*top black traces*) to a family of long current steps (*bottom traces*). Superimposed *magenta* traces show the responses to current steps of the same magnitude in an active compartmental model of the same octopus cell. (**c**) Somatic EPSP in response to a sweep of 0.6-ms duration from a typical passive model (*yellow*), active model (*magenta*), active model with spatially randomized inputs (*blue*), and a passive point model (*green*). (**d**) A comparison of the shape parameters between models for a sweep duration of 0.6 ms. *Color* scheme same as in panel (**c**). Statistical comparisons are in Table 3 of McGinley et al. (McGinley et al. 2012). Panels (**a**) and (**b**) are reproduced with permission from Fig. 14.2, panel (**c**) from Fig. 14.3, and panel (**d**) from Fig. 14.4 of ref. McGinley et al. (2012)

"input normalization" was discovered and thought to be important for reducing the location dependence of synaptic efficacy in hippocampal pyramidal neurons (Magee and Cook 2000). Surprisingly, input normalization had no effect on the dependence of somatic EPSP shape on somatopetal sweep duration (ref. McGinley et al. 2012, Fig. 14.3).

In active and passive models, somatopetal sweeps of activation lasting 0.6 ms—approximately equal to the duration expected in each octopus cell from the traveling wave delay—resulted in somatic EPSPs that were tall and sharp, and sharpest in active models (Fig. 14.3c, magenta and yellow curves). Responses in point models or passive models with randomized synaptic locations had smaller and more slowly rising EPSPs (Fig. 14.3c, blue and green curves). Active and passive models had short integration windows (the duration of the rising phase of the EPSP; ~0.2 and 0.3 ms, respectively), whereas randomized or point models had long integration windows (~0.5 ms; Fig. 14.3d, left). Thus, octopus cells are effective at compensating traveling wave delays in part due to their morphology and fast membranes.

14.5 The Role of Low-Voltage-Activated Potassium Channels

Although both active and passive models responded to sweeps matching the traveling wave delay with comparable rising rates and integration windows, half-widths were dramatically shorter in active than in passive models (0.5 vs. 1.2 ms; Fig. 14.3d, right). This reduction in half-width resulted from activation of g_{KL} channels during the EPSP, consistent with experimental observations in octopus cells and medial superior olivary neurons (Golding et al. 1999; Ferragamo and Oertel 2002; Svirskis et al. 2002; Scott et al. 2007). The large effect of g_{KL} channels on the falling phase of EPSPs is similar to the shortening of the falling phase of the action potential by potassium currents in classical and contemporary observations (Hodgkin et al. 1952; Bean 2007). The shortening of the falling phase of the EPSP by g_{KL} channels rapidly repolarizes EPSPs, which is important when they occur at high rates in the face of ongoing activity (Svirskis et al. 2004; Scott et al. 2007).

Activation of g_{KL} channels is also important in shaping the *rising* phase of the EPSP during somatopetal sweeps of activation in octopus cells. This can be seen in calculations of the sweep duration that results in the fastest rising and largest EPSP in passive versus active models. In active models, EPSPs were largest for sweeps lasting ~0.5 ms, with little variance between models (Fig. 14.4a, magenta symbol) in good agreement with the measured traveling wave delay of 0.53 ms per octopus cell (McGinley et al. 2012). Too slow of a sweep allows g_{KL} to activate and thereby reduce the EPSP amplitude. In passive models, however, the sweep duration with maximum EPSP amplitude varied between models from 0.8 to 1.6 ms (Fig. 14.4a, black symbol). Similarly, the rate of rise (dV/dt) of the EPSP was significantly larger in active than in passive models for physiological sweep durations; active models had a dV/dt of 50–70 mV/ms compared to 40–48 mV/ms in passive models for sweep durations of 0.4–0.6 ms (see ref. McGinley et al. 2012, Fig. 14.3b). The half-widths of EPSPs in passive and active models were similar to amplitudes in their dependence on sweep duration (Fig. 14.4a), further evidence of the role of g_{KL} in octopus cells' precise responses in the face of the cochlear traveling wave.
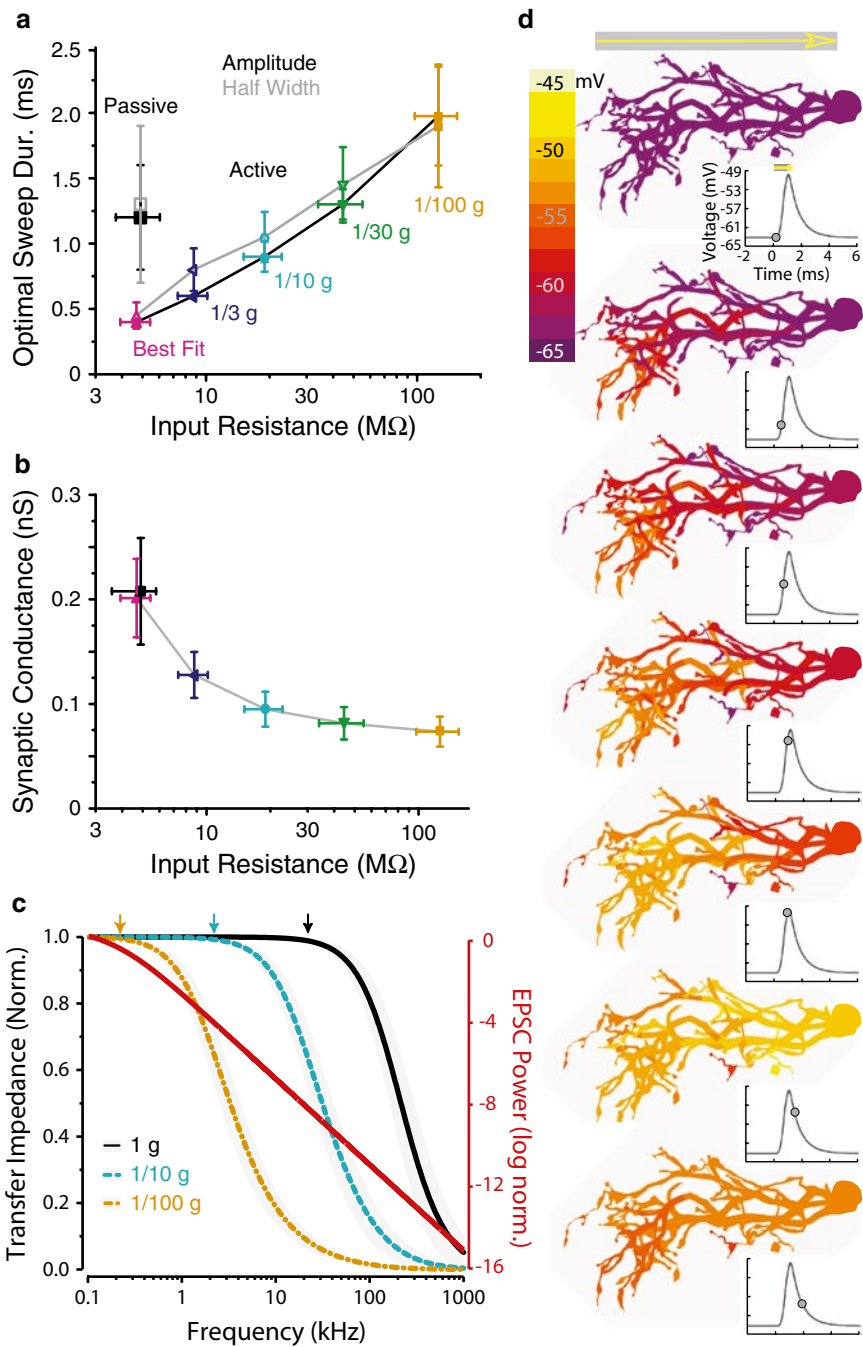
Fig. 14.4 Determinants of rapid signal transmission of octopus cells' dendrites. (**a**) The sweep duration that produces EPSPs with the largest amplitude or the narrowest half-width—the optimal sweep duration—is plotted against the input resistance for best-fit passive models (*black* and *grey squares*) and best-fit active models (*magenta triangles*) or active models with scaled membrane conductance (*other colored symbols*). *Black lines* and *filled symbols* are for amplitude; *grey lines*

14.6   Compensating Longer Delays in Low-Frequency-Hearing Animals

Octopus cells in mice have specialized dendritic morphology, connectivity, and biophysics tailored to compensate cochlear traveling wave delays and encode broadband transient sounds. However, several important aspects of octopus cell physiology remain unexplored, particularly relating to species with lower frequency hearing and thus longer traveling wave delays (Ruggero 1992; Ruggero and Rich 1987). Current findings motivate several possible mechanisms for octopus cells to compensate longer delays, including larger size, lower overall membrane conductance, lower dendritic g_{KL} conductance, or differences in the span of best frequencies in ANFs. Octopus cells in humans are large (Adams 1986). Octopus cells in cats and dogs have lower membrane conductance than in mice, but measurements have been made only in relatively immature animals (Bal and Baydas 2009; Bal et al. 2009).

The effect of overall membrane conductance on dendritic delay compensation was studied in active compartmental models of octopus cells (McGinley et al. 2012). Decreasing active and passive ion channel concentrations by 3-, 10-, 30-, or 100-fold changed the dendritic sweep duration that resulted in the largest and sharpest EPSPs over a range from 0.5 to 2.0 ms (Fig. 14.4a). Surprisingly, somatic input resistance changed only 25-fold, and the necessary synaptic conductance to elicit a large EPSP changed only 3-fold with the 100-fold change in ion channel concentration (Fig. 14.4b), demonstrating the importance of cytoplasmic resistance in dendritic integration. Bigger animals could use larger diameter dendrites to overcome cytoplasmic resistivity. Channels for g_{KL} have an ~3-fold lower density in the dendrites of MSO neurons (Mathews et al. 2010). Octopus cells might use a similar conductance gradient to compensate longer delays. However, changing the dendritic-to-somatic leak conductance over a 10,000-fold range had little effect on dendritic delay compensation in passive octopus cell models (see Fig. 7 of ref. McGinley et al. 2012). The role of conductance gradients of active channels in dendritic delay compensation should be studied further.

Fig. 14.4 (continued) and *open symbols* are for half-width. Conductance magnitudes for active models indicated below with colors matching the symbols. (**b**) The total synaptic conductance is plotted against the input resistance, for the same models as in panel A. To facilitate comparisons, the synaptic conductance for each cell in each model was adjusted so that the EPSP amplitude for zero sweep duration was 15 mV. (**c**) The transfer impedance in best-fit passive models (*black*) and passive models with 10-fold (*light blue*) or 100-fold (*orange*) reduced membrane conductance superimposed on the EPSC power spectrum plotted against frequency (*red*). *Arrows* indicate maximum frequency up to which each model has relatively constant transfer impedance. *Grey bands* indicate ±1 SD, calculated across models ($n=4$). (**d**) Color maps of the spatial profile of the voltage for a sweep duration of 0.6 ms in an example simulated passive octopus cell. The time corresponding to each color map is indicated on the simulated EPSP traces (*insets*) with a *green dot*. Panels (**a**) and (**b**) are reproduced with permission from Fig. 5 and panel (**d**) from Fig. 8 of ref. McGinley et al. (2012)

There is a trade-off between rapid membrane responsiveness and slow dendritic integration that limits the length of delays that octopus cells can compensate in their dendrites and still fire rapidly. Bushy cells in mice and octopus cells in immature cats and dogs have lower g_{KL} conductances resulting in lower dV/dt thresholds and thus less stringent coincident detection (McGinley and Oertel 2006; Bal and Baydas 2009; Bal et al. 2009). Octopus cells' low membrane resistance allows them to transmit fast synaptic signals down their dendrites. This can be seen by calculating the frequency dependence of the transfer impedance between the tips of the dendrites and the soma, using the ztransfer tool in NEURON (Hines and Carnevale 1997). Normalized transfer impedance values can be calculated by dividing by the value at 0.1 kHz in that model. In best-fit passive models of octopus cells, the normalized transfer impedance is flat up to ~20 kHz (Fig. 14.4c, black curve and arrow).

Thus, octopus cells' dendrites in mice transmit the frequency content in their excitatory postsynaptic currents (EPSCs) (Gardner et al. 1999). This can be seen in the power spectrum of a double-exponential fit to EPSC waveforms from the synaptic conductance, g_{syn} measured in octopus cells, which can be derived, and is

$$\mathrm{P}\left(f\right) = \frac{g_{max}^2 \times \left(w_f - w_r\right)^2}{\eta^2 \times \left(w_r^2 + f^2\right) \times \left(w_f^2 + f^2\right)},$$

where f is the frequency in kHz, $w = 1/\tau$, "r" and "d" refer to the rising and falling time constants of the double exponential, and η is a normalization factor, following ref. McGinley et al. (2012). Defining normalized EPSG power as $\log(\mathrm{P}(f)/P(0.1))$, where $P(0.1)$ is the power at 0.1 kHz, illustrates that the EPSC power spectrum in octopus cells is significant out to very high frequencies as a result of the extremely fast rise of the EPSC (Fig. 14.4c, red curve) (Gardner et al. 1999). When the conductance values in active models are divided by 10 (Fig. 14.4c, blue curve) or 100 (Fig. 14.4c, orange curve) while keeping all other parameters the same, they no longer reliably transfer the high-frequency components of EPSCs. For 10-fold reduction, the transfer impedance was flat up to ~2 kHz (Fig. 14.4c, blue arrow), and with 100-fold it was flat up to ~0.2 kHz (Fig. 14.4c, orange arrow). As a result of octopus cells' effective transfer of fast signals down their dendrites, a rapid somatopetal sweep of excitation results in progressive activation of the dendritic tree and rapidly rising EPSPs (Fig. 14.4d). The role of active conductances, particularly gKL, and conductance gradients in shaping the dendrite-to-soma transfer impedance warrants further exploration.

14.7 Downstream Processing and Comparison to Other Systems

Octopus cells are perhaps the fastest dendritic integrators in the brain (Golding and Oertel 2012; McGinley et al. 2012; McGinley and Oertel 2006; Oertel et al. 2000, 2009; Spruston et al. 2007) and encode sounds with extraordinary temporal

precision (Godfrey et al. 1975; Oertel et al. 2000; Rhode 1994, 1998; Rhode and Smith 1986). Yet, our understanding of how this exquisite spectro-temporal processing is utilized by downstream circuits is based on indirect evidence and speculation. Octopus cells project predominantly to the contralateral ventral subdivision of the ventral nucleus of the lateral lemniscus (VNLLv) with exceptionally thick axons (Adams 1997; Smith et al. 2005; Schofield and Cant 1997) where they form large endbulb endings onto somas (Adams 1997; Vater and Feng 1990). This configuration results in rapid and powerful excitation of their targets (Schofield and Cant 1997; Vater and Feng 1990; Willard and Ryugo 1983), which are similar morphologically—and perhaps physiologically—to the temporally precise large spherical bushy cells in the VCN (Adams 1997; Wu 1999; McGinley and Oertel 2006; Oertel et al. 2009). VNLLv spherical bushy cells are inhibitory neurons (Saint Marie et al. 1997; Moore and Moore 1987; Winer et al. 1995) and project predominantly non-topographically to the ipsilateral inferior colliculus (IC) (Adams 1979; Brunso-Bechtold et al. 1981; Roth et al. 1978; Whitley and Henkel 1984; Loftus et al. 2010).

Consistent with anatomical predictions, neurons in the VNLL synchronize to rapid sound modulations (Zhang and Kelly 2006). Some neurons in VNLL respond to clicks with large-amplitude, short-duration, onset inhibition, probably further sharpening the output to IC (Nayagam et al. 2005). There is substantial physiological evidence of rapid and broadly tuned inhibition in the IC. Short latency inhibition is seen in a large fraction of unit responses in the IC of cats and rabbits to a wide range of sounds, particularly when unanesthetized (Kuwada et al. 1989; Carney and Yin 1989; Fitzpatrick et al. 1995, 1999; Bock et al. 1972). Pharmacological evidence supports that short latency inhibition is a direct GABAergic or glycinergic input to the IC (Casseday et al. 2000). Rapid and/or side-band hyperpolarization of the membrane potential plays a key role in response area of many intracellularly recorded IC neurons (Kuwada et al. 1997). Much of this rapid and broadband input could be driven by the octopus cell-to-VNLL pathway. However, broadly tuned inputs to the central nucleus of IC, including from the DNLL and elsewhere in the VNLL, are also inhibitory, possibly because broadband excitation would degrade the tonotopic organization (Oertel and Wickesberg 2002).

The temporally precise disynaptic inhibitory pathway from octopus cells, through the VNLL, to the IC may be preserved from birds and reptiles, through rodents, bats, and cats, to humans (Adams 1979, 1997; Carr and Code 2000), and yet its function is unknown. It has been hypothesized that the function relates to pattern recognition in natural sounds (Oertel and Wickesberg 2002). Alternatively, the pathway could serve to sharpen tonotopy in the IC by providing lateral inhibition (Blakemore et al. 1970), though it is not clear why extraordinary speed would be necessary for this purpose (Amari 1977). Instead, the disynaptic inhibitory pathway could aid in sound source separation or stream segregation (Bregman 1994) by "wiping the slate" of activity in IC neurons at the initiation of sounds, providing a signal for "binding" immediately subsequent activity into a percept (Treisman 1996; Shadlen and Movshon 1999). This binding mechanism could contribute to the precedence effect (Langner 1992; Litovsky et al. 1999) and echo suppression (Yin 1994), because the first instance of the sound would usually contain the

sharpest onsets and thus engage the binding mechanism most strongly. The disynaptic pathway likely contributes to transforming the rapid temporal code in the auditory periphery into a rate code or a slower temporal code in the IC suitable for processing by thalamocortical circuits (Eggermont 2001; Joris et al. 2004).

Octopus cells compensate the cochlear traveling wave delay using sensitivity to somatopetal sweeps of excitation, with passive cable properties playing a significant role. Thus, octopus cells may be the clearest example to date of a computation performed using Rall's prediction in 1964 of dendritic sensitivity to sweeps (Rall 1964). Some amacrine and ganglion cells in the retina use sensitivity to dendritic sweeps to compute object motion (Euler et al. 2002; Vaney et al. 2012). However, motion occurs over a wide range of temporal and spatial scales, and thus multiple complex circuit, synaptic, and intrinsic mechanisms play a role in this computation (Briggman et al. 2011; Vaney et al. 2012; Chap. 13 in this book). It has been demonstrated that cortical neurons are sensitive to sweeps of excitation, possibly to aid in detection of temporal input sequences (Branco et al. 2010; Chap. 15 in this book). However, sweep sensitivity in cortical neurons occurs on a much slower time scale than in octopus cells, supported by impedance gradients and other nonlinearities in cortical dendrites (Branco et al. 2010). Given the primitive state of our understanding of the precise distribution of ion channels in dendrites and the in vivo patterns of dendritic activation in most brain areas (Briggman et al. 2011; Bock et al. 2011; Johnston and Narayanan 2008), dendritic sweep sensitivity—predicted by Rall and exploited elegantly by octopus cells—will be the subject of study for decades to come.

References

Adams JC (1979) Ascending projections to the inferior colliculus. J Comp Neurol 183(3):519–538

Adams JC (1986) Neuronal morphology in the human cochlear nucleus. Arch Otolaryngol Head Neck Surg 112(12):1253

Adams J (1997) Projections from octopus cells of the posteroventral cochlear nucleus to the ventral nucleus of the lateral lemniscus in cat and human. Aud Neurosci 3(4):335–350

Agmon-Snir H, Segev I (1993) Signal delay and input synchronization in passive dendritic structures. J Neurophysiol 70(5):2066–2085

Amari S (1977) Dynamics of pattern formation in lateral-inhibition type neural fields. Biol Cybern 27(2):77–87

Bal R, Baydas G (2009) Electrophysiological properties of octopus neurons of the cat cochlear nucleus: an in vitro study. J Assoc Res Otolaryngol 10(2):281–293

Bal R, Oertel D (2000) Hyperpolarization-activated, mixed-cation current (I h) in octopus cells of the mammalian cochlear nucleus. J Neurophysiol 84(2):806–817

Bal R, Oertel D (2001) Potassium currents in octopus cells of the mammalian cochlear nucleus. J Neurophysiol 86(5):2299–2311

Bal R, Oertel D (2007) Voltage-activated calcium currents in octopus cells of the mouse cochlear nucleus. J Assoc Res Otolaryngol 8(4):509–521

Bal R, Baydas G, Naziroglu M (2009) Electrophysiological properties of ventral cochlear nucleus neurons of the dog. Hear Res 256(1):93–103

Bean BP (2007) The action potential in mammalian central neurons. Nat Rev Neurosci 8(6):451–465

Bendor D, Wang X (2005) The neuronal representation of pitch in primate auditory cortex. Nature 436(7054):1161–1165

Blakemore C, Carpenter RH, Georgeson MA (1970) Lateral inhibition between orientation detectors in the human visual system. Nature 228:37–39

Bock G, Webster W, Aitkin L (1972) Discharge patterns of single units in inferior colliculus of the alert cat. J Neurophysiol 35:265–277

Bock DD, Lee WCA, Kerlin AM, Andermann ML, Hood G, Wetzel AW, Yurgenson S, Soucy ER, Kim HS, Reid RC (2011) Network anatomy and in vivo physiology of visual cortical neurons. Nature 471(7337):177–182

Branco T, Clark B, Häusser M (2010) Dendritic discrimination of temporal input sequences in cortical neurons. Science 329(5999):1671–1675

Bregman AS (1994) Auditory scene analysis: the perceptual organization of sound. MIT Press, Cambridge

Briggman KL, Helmstaedter M, Denk W (2011) Wiring specificity in the direction-selectivity circuit of the retina. Nature 471(7337):183–188

Brunso-Bechtold J, Thompson G, Masterton R (1981) HRP study of the organization of auditory afferents ascending to central nucleus of inferior colliculus in cat. J Comp Neurol 197(4):705–722

Cai Y, Walsh EJ, McGee JA (1997) Mechanisms of onset responses in octopus cells of the cochlear nucleus: implications of a model. J Neurophysiol 78(2):872–883

Cai Y, McGee JA, Walsh EJ (2000) Contributions of ion conductances to the onset responses of octopus cells in the ventral cochlear nucleus: simulation results. J Neurophysiol 83(1):301–314

Cao XJ, Oertel D (2011) The magnitudes of hyperpolarization-activated and low-voltage-activated potassium currents co-vary in neurons of the ventral cochlear nucleus. J Neurophysiol 106(2):630–640

Carney LH, Yin T (1989) Responses of low-frequency cells in the inferior colliculus to interaural time differences of clicks: excitatory and inhibitory components. J Neurophysiol 62(1):144–161

Carr CE, Code RA (2000) The central auditory system of reptiles and birds. Comparative hearing: birds and reptiles. Springer, New York, pp 197–248

Casseday JH, Ehrlich D, Covey E (2000) Neural measurement of sound duration: control by excitatory–inhibitory interactions in the inferior colliculus. J Neurophysiol 84(3):1475–1487

Dallos P (1992) The active cochlea. J Neurosci 12(12):4575–4585

Eggermont JJ (2001) Between sound and perception: reviewing the search for a neural code. Hear Res 157(1):1–42

Euler T, Detwiler PB, Denk W (2002) Directionally selective calcium signals in dendrites of starburst amacrine cells. Nature 418(6900):845–852

Ferragamo MJ, Oertel D (2002) Octopus cells of the mammalian ventral cochlear nucleus sense the rate of depolarization. J Neurophysiol 87(5):2262–2270

Fitzpatrick DC, Kuwada S, Batra R, Trahiotis C (1995) Neural responses to simple simulated echoes in the auditory brain stem of the unanesthetized rabbit. J Neurophysiol 74(6):2469–2486

Fitzpatrick DC, Kuwada S, Kim D, Parham K, Batra R (1999) Responses of neurons to click-pairs as simulated echoes: auditory nerve to auditory cortex. J Acoust Soc Am 106:3460

Gabor M (1946) Theory of Communication. J Inst Elec Eng 93:429–457

Gardner SM, Trussell LO, Oertel D (1999) Time course and permeation of synaptic AMPA receptors in cochlear nuclear neurons correlate with input. J Neurosci 19(20):8721–8729

Gardner SM, Trussell LO, Oertel D (2001) Correlation of AMPA receptor subunit composition with synaptic input in the mammalian cochlear nuclei. J Neurosci 21(18):7428–7437

Godfrey DA, Kiang N, Norris BE (1975) Single unit activity in the posteroventral cochlear nucleus of the cat. J Comp Neurol 162(2):247–268

Golding NL, Oertel D (2012) Synaptic integration in dendrites: exceptional need for speed. J Physiol 590:5563–5569

Golding NL, Robertson D, Oertel D (1995) Recordings from slices indicate that octopus cells of the cochlear nucleus detect coincident firing of auditory nerve fibers with temporal precision. J Neurosci 15(4):3138–3153

Golding NL, Ferragamo MJ, Oertel D (1999) Role of intrinsic conductances underlying responses to transients in octopus cells of the cochlear nucleus. J Neurosci 19(8):2897–2905

Heisenberg W (1927) Über den anschaulichen inhalt der quantentheoretischen kinematik und mechanik. Zeitschrift Für Physik 43(3–4):172–198

Hille B (1994) Modulation of ion-channel function by G-protein-coupled receptors. Trends Neurosci 17(12):531–536

Hines ML, Carnevale NT (1997) The NEURON simulation environment. Neural Comput 9(6):1179–1209

Hodgkin AL, Huxley AF, Katz B (1952) Measurement of current–voltage relations in the membrane of the giant axon of Loligo. J Physiol 116(4):424

Johnston D, Narayanan R (2008) Active dendrites: colorful wings of the mysterious butterflies. Trends Neurosci 31(6):309–316

Joris P, Schreiner C, Rees A (2004) Neural processing of amplitude-modulated sounds. Physiol Rev 84(2):541–577

Khurana S, Remme MWH, Rinzel J, Golding NL (2011) Dynamic interaction of Ih and IK-LVA during trains of synaptic potentials in principal neurons of the medial superior olive. J Neurosci 31(24):8936–8947

Kirkpatrick S, Vecchi M (1983) Optimization by simmulated annealing. Science 220(4598):671–680

Kolston J, Osen K, Hackney C, Ottersen O, Storm-Mathisen J (1992) An atlas of glycine-and GABA-like immunoreactivity and colocalization in the cochlear nuclear complex of the guinea pig. Anat Embryol 186(5):443–465

König P, Engel AK, Singer W (1996) Integrator or coincidence detector? The role of the cortical neuron revisited. Trends Neurosci 19(4):130

Kuwada S, Batra R, Stanford TR (1989) Monaural and binaural response properties of neurons in the inferior colliculus of the rabbit: effects of sodium pentobarbital. J Neurophysiol 61(2):269–282

Kuwada S, Batra R, Yin TCT, Oliver DL, Haberly LB, Stanford TR (1997) Intracellular recordings in response to monaural and binaural stimulation of neurons in the inferior colliculus of the cat. J Neurosci 17(19):7565–7581

Langner G (1992) Periodicity coding in the auditory system. Hear Res 60(2):115–142

Lanzinger DJ (1987) Group delay caused by impedance mismatch. In ARFTG Conference Digest-Spring, 29th. IEEE 11:247–264

Levy KL, Kipke DR (1998) Mechanisms of the cochlear nucleus octopus cell's onset response: synaptic effectiveness and threshold. J Acoust Soc Am 103:1940

Litovsky RY, Colburn HS, Yost WA, Guzman SJ (1999) The precedence effect. J Acoust Soc Am 106(4):1633–1654

Loftus WC, Bishop DC, Oliver DL (2010) Differential patterns of inputs create functional zones in central nucleus of inferior colliculus. J Neurosci 30(40):13396–13408

Magee JC, Cook EP (2000) Somatic EPSP amplitude is independent of synapse location in hippocampal pyramidal neurons. Nat Neurosci 3:895–903

Marie RLS, Morest DK, Brandon CJ (1989) The form and distribution of GABAergic synapses on the principal cell types of the ventral cochlear nucleus of the cat. Hear Res 42(1):97–112

Mathews PJ, Jercog PE, Rinzel J, Scott LL, Golding NL (2010) Control of submillisecond synaptic timing in binaural coincidence detectors by Kv1 channels. Nat Neurosci 13(5):601–609

McGinley MJ, Oertel D (2006) Rate thresholds determine the precision of temporal integration in principal cells of the ventral cochlear nucleus. Hear Res 216:52–63

McGinley MJ, Lazimy YM, Bal R, Oertel D (2005) Measurement and modeling of cable properties and optimal input delay profiles in octopus cells of the ventral cochlear nucleus. Ass Res Otolaryngol 28

McGinley MJ, Liberman MC, Bal R, Oertel D (2012) Generating synchrony from the asynchronous: compensation for cochlear traveling wave delays by the dendrites of individual brainstem neurons. J Neurosci 32(27):9301–9311

Mills AW (1958) On the minimum audible angle. J Acoust Soc Am 30(4):237–246

Moore JK, Moore RY (1987) Glutamic acid decarboxylase-like immunoreactivity in brainstem auditory nuclei of the rat. J Comp Neurol 260(2):157–174

Morest DK, Kiang NYS, Kane EC, Guinan Jr J, Godfrey D (1973) Stimulus coding at caudal levels of the cat's auditory nervous system. II. Patterns of synaptic organization (Moller AR and Boston P., eds.) New York Academic, 479–504

Morley BJ, Happe HK (2000) Cholinergic receptors: dual roles in transduction and plasticity. Hear Res 147(1):104–112

Nayagam DAX, Clarey JC, Paolini AG (2005) Powerful, onset inhibition in the ventral nucleus of the lateral lemniscus. J Neurophysiol 94(2):1651–1654

Oertel D, Wickesberg RE (2002) Ascending pathways through ventral nuclei of the lateral lemniscus and their possible role in pattern recognition in natural sounds. Integrative functions in the mammalian auditory pathway. Springer Verlag, New York, pp 207–237

Oertel D, Bal R, Gardner SM, Smith PH, Joris PX (2000) Detection of synchrony in the activity of auditory nerve fibers by octopus cells of the mammalian cochlear nucleus. Proc Natl Acad Sci USA 97(22):11773–11779

Oertel D, Shatadal S, Cao X-J (2008) In the ventral cochlear nucleus Kv1. 1 and subunits of HCN1 are colocalized at surfaces of neurons that have low-voltage-activated and hyperpolarization-activated conductances. Neurosci 154(1):77–86

Oertel D, McGinley MJ, Cao XJ (2009) Temporal processing in the auditory pathway. Encyclopedia Neurosci 9:909–919

Osen KK (1969) Cytoarchitecture of the cochlear nuclei in the cat. J Comp Neurol 136(4):453–483

Osen K (1970) Course and termination of the primary afferents in the cochlear nuclei of the cat. An experimental anatomical study. Arch Ital Biol 108(1):21

Rall W (1964) Theoretical significance of dendritic trees for neuronal input–output relations. In: Reiss RF (ed) Neural theory and modeling. Stanford Univ. Press, Stanford, CA

Raman IM, Trussell LO (1992) The kinetics of the response to glutamate and kainate in neurons of the avian cochlear nucleus. Neuron 9(1):173–186

Rhode WS (1994) Temporal coding of 200 % amplitude modulated signals in the ventral cochlear nucleus of cat. Hear Res 77(1):43–68

Rhode WS (1995) Interspike intervals as a correlate of periodicity pitch in cat cochlear nucleus. J Acoust Soc Am 97(4):2414

Rhode WS (1998) Neural encoding of single-formant stimuli in the ventral cochlear nucleus of the chinchilla. Hear Res 117(1–2):39

Rhode WS, Smith PH (1986) Encoding timing and intensity in the ventral cochlear nucleus of the cat. J Neurophysiol 56(2):261–286

Rhode W, Oertel D, Smith P (1983) Physiological response properties of cells labeled intracellularly with horseradish peroxidase in cat ventral cochlear nucleus. J Comp Neurol 213(4):448–463

Roth G, Aitkin L, Andersen R, Merzenich M (1978) Some features of the spatial organization of the central nucleus of the inferior colliculus of the cat. J Comp Neurol 182(4):661–680

Ruggero MA (1992) Responses to sound of the basilar membrane of the mammalian cochlea. Curr Opin Neurobiol 2(4):449–456

Ruggero MA, Rich NC (1987) Timing of spike initiation in cochlear afferents: dependence on site of innervation. J Neurophysiol 58(2):379–403

Saint Marie RL, Shneiderman A, Stanforth DA (1997) Patterns of γ-aminobutyric acid and glycine immunoreactivities reflect structural and functional differences of the cat lateral lemniscal nuclei. J Comp Neurol 389(2):264–276

Schofield BR, Cant NB (1997) Ventral nucleus of the lateral lemniscus in guinea pigs: cytoarchitecture and inputs from the cochlear nucleus. J Comp Neurol 379(3):363–385

Scott LL, Mathews PJ, Golding NL (2005) Posthearing developmental refinement of temporal processing in principal neurons of the medial superior olive. J Neurosci 25(35):7887–7895

Scott LL, Hage TA, Golding NL (2007) Weak action potential backpropagation is associated with high-frequency axonal firing capability in principal neurons of the gerbil medial superior olive. J Physiol 583(2):647–661

Shadlen MN, Movshon JA (1999) Synchrony unbound: review a critical evaluation of the temporal binding hypothesis. Neuron 24:67–77

Smith PH, Massie A, Joris PX (2005) Acoustic stria: anatomy of physiologically characterized cells and their axonal projection patterns. J Comp Neurol 482(4):349–371

Spencer MJ, Grayden DB, Bruce IC, Meffin H, Burkitt AN (2012) An investigation of dendritic delay in octopus cells of the mammalian cochlear nucleus. Front Comput Neurosci 6:83

Spruston N, Stuart G, Häusser M (2007) Dendritic integration. Dendrites. eds. Oxford University Press. 231–271

Svirskis G, Kotak V, Sanes DH, Rinzel J (2002) Enhancement of signal-to-noise ratio and phase locking for small inputs by a low-threshold outward current in auditory neurons. J Neurosci 22(24):11019–11025

Svirskis G, Kotak V, Sanes DH, Rinzel J (2004) Sodium along with low-threshold potassium currents enhance coincidence detection of subthreshold noisy signals in MSO neurons. J Neurophysiol 91(6):2465–2473

Szentagothai J, Arbib MA (1974) Conceptual models of neural organization. Neurosci Res Program Bull 12:305–510

Taberner AM, Liberman MC (2005) Response properties of single auditory nerve fibers in the mouse. J Neurophysiol 93(1):557–569

Treisman A (1996) The binding problem. Curr Opin Neurobiol 6(2):171–178

Vaney DI, Sivyer B, Taylor WR (2012) Direction selectivity in the retina: symmetry and asymmetry in structure and function. Nat Rev Neurosci 13:194–208

Vater M, Feng AS (1990) Functional organization of ascending and descending connections of the cochlear nucleus of horseshoe bats. J Comp Neurol 292(3):373–395

Weisburn BA, Parks, TW (1992) Cochlear filters: resolution and the uncertainty principle. In: Digital signal processing workshop, 1992. The (pp. 1–6). IEEE

Wenthold R, Huie D, Altschuler R, Reeks K (1987) Glycine immunoreactivity localized in the cochlear nucleus and superior olivary complex. Neurosci 22(3):897–912

Whitley JM, Henkel CK (1984) Topographical organization of the inferior collicular projection and other connections of the ventral nucleus of the lateral lemniscus in the cat. J Comp Neurol 229(2):257–270

Wickesberg RE, Oertel D (1988) Tonotopic projection from the dorsal to the anteroventral cochlear nucleus of mice. J Comp Neurol 268(3):389–399

Wickesberg RE, Whitlon D, Oertel D (1991) Tuberculoventral neurons project to the multipolar cell area but not to the octopus cell area of the posteroventral cochlear nucleus. J Comp Neurol 313(3):457–468

Wickesberg RE, Whitlon D, Oertel D (1994) In vitro modulation of somatic glycine-like immunoreactivity in presumed glycinergic neurons. J Comp Neurol 339(3):311–327

Willard FH, Ryugo DK (1983) Anatomy of the central auditory system. The auditory psychobiology of the mouse. Springfield: CC Thomas. p 201–304

Winer JA, Larue DT, Pollak GD (1995) GABA and glycine in the central auditory system of the mustache bat: structural substrates for inhibitory neuronal organization. J Comp Neurol 355(3):317–353

Wu SH (1999) Synaptic excitation in the dorsal nucleus of the lateral lemniscus. Prog Neurobiol 57(3):357–375

Yang X, Wang K, Shamma SA (1992) Auditory representations of acoustic signals. IEEE Transactions on information. Theory 38(2):824–839

Yin T (1994) Physiological correlates of the precedence effect and summing localization in the inferior colliculus of the cat. J Neurosci 14(9):5170–5186

Zhang H, Kelly JB (2006) Responses of neurons in the rat's ventral nucleus of the lateral lemniscus to amplitude-modulated tones. J Neurophysiol 96(6):2905–2914